Received 11 March 2021; accepted 28 March 2021. Date of publication 31 March 2021; date of current version 12 April 2021.
The review of this paper was arranged by Editor S. Chakrabarti.

Digital Object Identifier 10.1109/JEDS.2021.3069973

Fabrication and Characterization of GaN-Based Fin-Channel Array Metal-Oxide-Semiconductor High-Electron Mobility Transistors With Recessed-Gate and Ga_2O_3 Gate Insulator Layer

HSIN-YING LEE [1] (Member, IEEE), TING-WEI CHANG [2], EDWARD YI CHANG [3] (Fellow, IEEE), NIKLAS RORSMAN [4], AND CHING-TING LEE [1,2,5] (Life Fellow, IEEE)

1 Department of Photonics, National Cheng Kung University, Tainan 701, Taiwan
2 Institute of Microelectronics, Department of Electrical Engineering, National Cheng Kung University, Tainan 701, Taiwan
3 Department of Materials Science and Engineering, National Yang Ming Chiao Tung University, Hsinchu 300, Taiwan
4 Department of Microtechnology and Nanoscience, Chalmers University of Technology, 412 96 Gothenburg, Sweden
5 Department of Electrical Engineering, Yuan Ze University, Taoyuan 320, Taiwan

CORRESPONDING AUTHOR: Ching-Ting Lee (e-mail: ctlee@ee.ncku.edu.tw)

This work was supported in part by the Ministry of Science and Technology of the Republic of China under Grant MOST 108-2221-E-155-029-MY3, Grant MOST 108-2221-E-006-215-MY3, and Grant MOST 109-2923-E-155-001; and in part by the Swedish Strategic research Foundation under Contract STP19-0008.

ABSTRACT In this work, the properties of gallium oxide (Ga_2O_3) and its excellent interface properties to GaN-based materials are explored as a gate insulator layer for GaN-based metal-oxide-semiconductor high-electron mobility transistors (MOSHEMTs). A novel vapor cooling condensation system was used to deposit the high quality Ga_2O_3 films with high insulation and low defect suitable for gate insulator layer. The characteristics of the Ga_2O_3 films were further explored by implementing GaN-based fin-channel array MOSHEMTs with recessed-gates and different channel widths. Compared to planar channel structure, the direct current, high frequency, and flicker noise performances were enhanced in the fin-channel MOSHEMTs with Ga_2O_3 gate insulator layer. For the GaN-based fin-channel array MOSHEMTs with 300-nm-wide channel, the devices exhibited superior performances of maximum extrinsic transconductance of 194.2 mS/mm, threshold voltage of −1.4 V, extrinsic unit gain cutoff frequency of 6.4 GHz, maximum oscillation frequency of 14.8 GHz, and normalized noise power of 8.45×10^{-15} Hz^{-1}. It was also demonstrated that the associated performances were improved by reducing the width of fin-channel array.

INDEX TERMS Ga_2O_3 gate insulator layer, GaN-based MOSHEMTs, laser interference photolithography system, fin-channel array, vapor cooling condensation system.

I. INTRODUCTION

GaN-based high-electron mobility transistors (HEMTs) are suitable for high temperature, high power, and high frequency applications [1], [2], due to wide bandgap as well as good electron transport properties and high sheet electron density of two-dimensional electron gas (2-DEG) residing in the available heterostructures of the material system. Despite impressive performances of GaN-based metal-semiconductor high-electron mobility transistors (MESHEMTs), metal-oxide-semiconductor high-electron mobility transistors (MOSHEMTs) have more recently attracted interest to improve the high voltage operation and high power-handling capability. Several dielectric materials have been used as gate insulator by inserting them between the GaN-based semiconductors and gate metals [3]–[5]. Owing to the high radiation resistance,

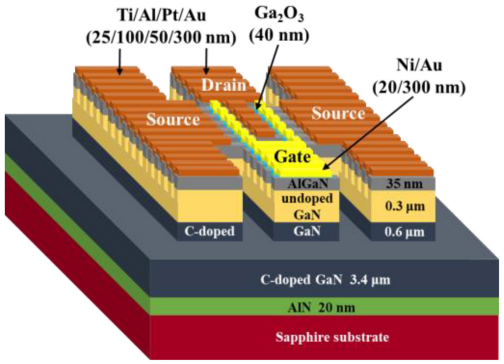

FIGURE 1. Epitaxial layers and schematic configuration of GaN-based fin-MOSHEMTs.

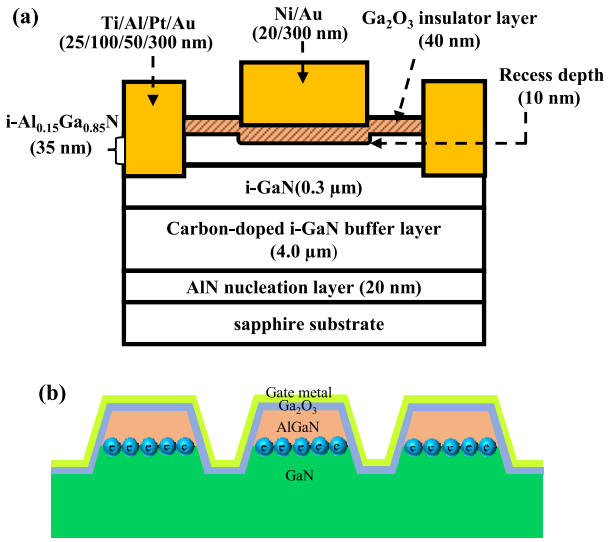

FIGURE 2. Cross-sectional configuration of (a) source, gate, and drain regions and (b) fin-channel array.

high breakdown electric field, high thermal stability, and high chemical stability of Ga_2O_3 material [6], it has previously been used in electronic devices and electrooptical devices [7]–[9]. Furthermore, the Ga_2O_3 material is expected to be a good gate insulator for GaN-based MOSHEMTs, since the Ga_2O_3/GaN interface exhibits superior interface properties caused by the spontaneous termination of Ga-atoms with oxygen [10]. Although several methods have been used to deposit Ga_2O_3 thin films [11]–[13], it is difficult to obtain the required insulator properties due to the undesirably induced oxygen vacancies and defects residing within the Ga_2O_3 thin films [14].

In this work, we apply the vapor cooling condensation system to deposit high quality Ga_2O_3 thin films as the gate-insulator in various GaN-based fin-MOSHEMTs. The direct current (DC), high frequency, and low frequency noise performances of the resulting GaN-based planar channel and fin-submicron channel array MOSHEMTs with Ga_2O_3 gate insulator layer were measured and analyzed.

II. EXPERIMENT

A metalorganic chemical vapor deposition (MOCVD) system was used to grow epitaxial layers of GaN-based MOSHEMTs on c-plane sapphire substrates. The epitaxial layers included a 20-nm-thick AlN nucleation layer, 4.0-μm-thick carbon-doped GaN buffer layer, 300-nm-thick undoped i-GaN layer, and 35-nm-thick $Al_{0.15}Ga_{0.85}N$ layer (referred to as AlGaN, hereafter). The induced 2-DEG electron density and mobility were 1.11×10^{13} cm^{-2} and 1700 cm^2/V-s, respectively.

Fig. 1 shows the epitaxial layers and schematic configuration of the GaN-based fin-MOSHEMT consisting of an array of submicron channels with Ga_2O_3 gate insulator layer and recessed-gates. The fin-channels were defined with a He-Cd laser interference photolithography system using AZ6112 positive photoresist. By changing the incident angle of the two-intersected He-Cd laser beams, both 300-nm-wide and 500-nm-wide channel arrays were defined. After a lift-off process, a Ni/Au (20/100 nm) mask was formed. A photoelectrochemical (PEC) etching method was used to etch the unmasked AlGaN regions to a depth of about 70 nm. The PEC etching system was reported previously [15]. Standard photolithography system and reactive-ion-etching system were sequentially used to define and form the mesa isolation region (310 μm $\times$ 320 μm) using a Ni (500 nm) mask. After removing the native oxide on the AlGaN surface with an $(NH_4)_2S_x$ solution at 60 °C for 30 min [16], source and drain electrodes were formed by evaporating Ti/Al/Pt/Au (25/100/50/300 nm) metals and annealing in a N_2 ambient rapid-thermal-annealing (RTA) system at 800 °C for 2 min. Using the measurement of a transfer length method, the resulting specific contact resistance was about 7.0×10^{-6} Ω-cm^2. The separation between source electrode and drain electrode was 6 μm. Using standard photolithography to define gate-recessed structure, the 10-nm-deep and 1-μm-wide gate-recessed regions were etched with a PEC etching system. The vapor cooling condensation system [17] was used to deposit 40-nm-thick Ga_2O_3 layer as the gate insulator layer at approximately 80 K. The sample was then annealed in an oxygen ambience at 900 °C for 60 min. Using the measurement of X-ray diffraction pattern, the as-deposited Ga_2O_3 films were amorphous and the 900 °C-annealed Ga_2O_3 films were polycrystalline β-Ga_2O_3 films [18]. The electron concentration of 1.0×10^{15} cm^{-3} and electron mobility of 16.0 cm^2/V-s of the resulting Ga_2O_3 insulator layer were obtained previously [18]. 1-μm-wide Ni/Au (20/320 nm) gate metals were deposited using an electron-beam evaporator system and a lift-off process. The gate with 1 μm length was located at the center regions between source electrode and drain electrode and the gate-to-drain separation was 2.5 μm. Fig. 2(a) and Fig. 2(b) show the cross-sectional configuration of source, gate, and drain regions, and its cross-sectional configuration of a fin-channel array, respectively.

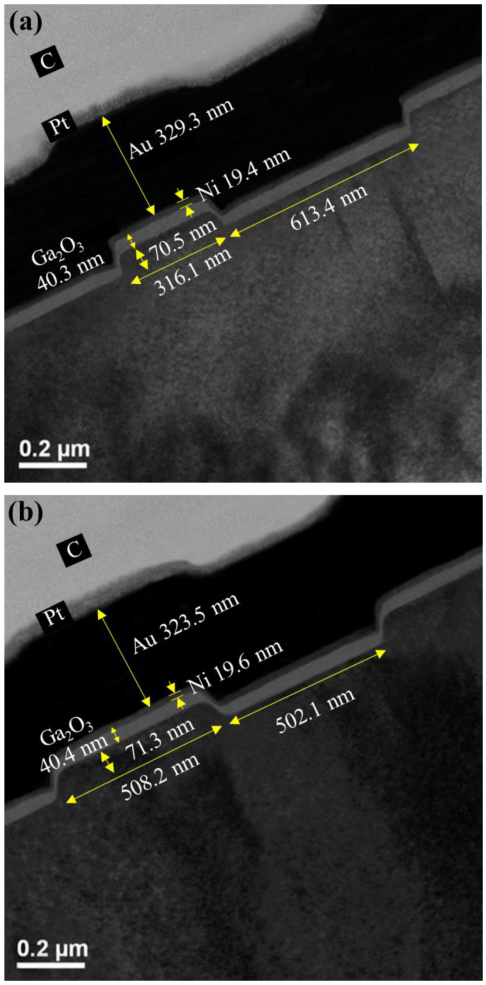

FIGURE 3. High resolution transmission electron microscopy image of cross-sectional configuration of (a) 300-nm-wide fin-channel array and (b) 500-nm-wide fin-channel array.

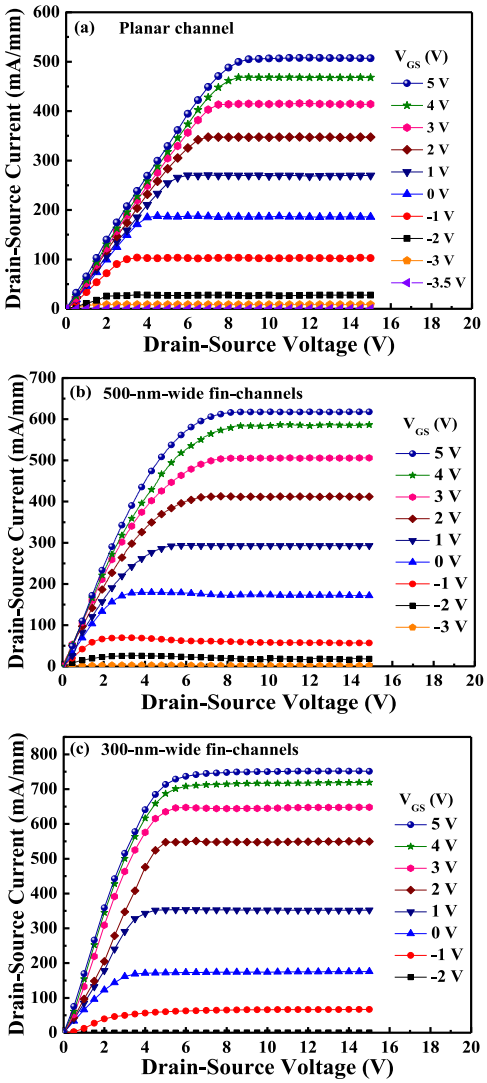

FIGURE 4. Typical drain-source current-drain-source voltage characteristics of AlGaN/GaN MOSHEMTs with (a) planar channel, (b) 500-nm-wide fin-channel array, and (c) 300-nm-wide fin-channel array.

III. EXPERIMENTAL RESULTS AND DISCUSSION

Fig. 3(a) shows the high resolution transmission electron microscopy (HRTEM) image of the cross-sectional AlGaN/GaN submicron fin-channel array MOSHEMTs with 300-nm-wide channels. In the HRTEM image, the Pt layer was deposited for protecting sample by ion bombardment during cutting process using focus ion beam system. Besides, the carbon (C) layer was deposited to protect sample during HRTEM measurement. The actual channel width and channel period were 316.1 nm and 929.5 nm, respectively. Consequently, there are 53 channels within the 50-μm-wide source electrode and drain electrode, resulting in a real total channel width of 16.75 μm. Fig. 3(b) shows the HRTEM image of the MOSHEMTs with 500-nm wide channels. In this case, the channel width, channel period, channel number and real total channel width were 508.2 nm, 1010.3 nm, 50, and 25.41 μm, respectively.

Figs. 4(a), (b), and (c) show the typical drain-source current-drain-source voltage (I_{DS}-V_{DS}) characteristics of the AlGaN/GaN MOSHEMTs with planar channel, 500-nm-wide channels, and 300-nm-wide channels, respectively. The normalized saturation drain-source current was 506.7 mA/mm, 617.6 mA/mm, and 750.0 mA/mm, respectively, at a bias of V_{DS} = 10 V and V_{GS} = 5 V. The normalized drain-source current was normalized by the associated real total channel width. The normalized saturation drain-source current increased with a reduction of channel width due to the better heat dissipation driven by lateral heat flow [19], [20]. Fig. 5 shows the associated drain-source current and extrinsic transconductance (g_m) as a function of gate-source voltage at V_{DS} = 10 V. A threshold voltage (V_T) of −3.5 V, −2.3 V, and −1.4 V was obtained for the devices with planar channel, 500-nm-wide channel array, and 300-nm-wide channel array, respectively. The reduction in absolute threshold voltage ($|V_T|$) with a narrower fin-channel width is attributed to the enhanced pinch-off effect

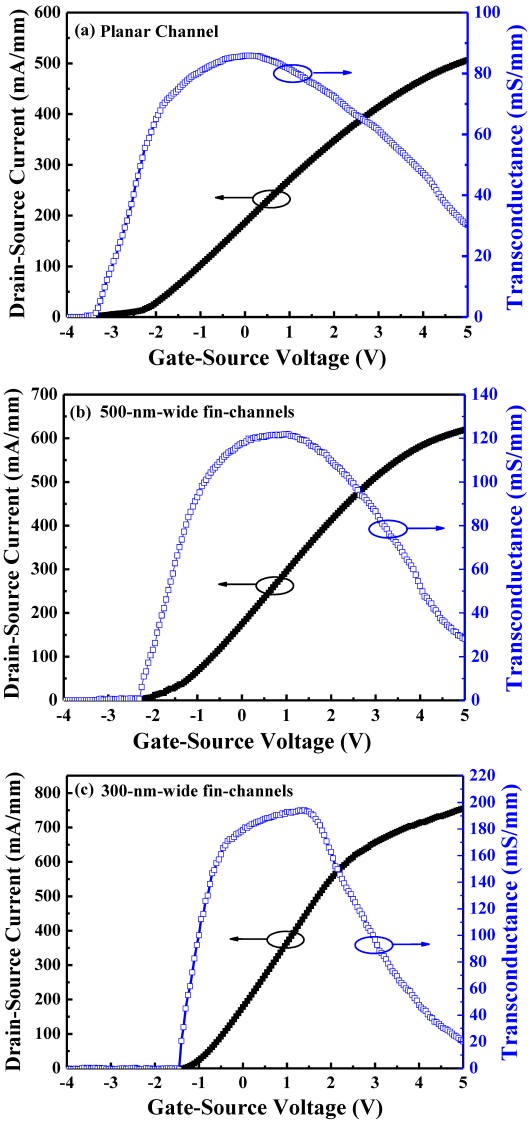

FIGURE 5. Drain-source current-gate-source voltage characteristics and extrinsic transconductance-gate-source voltage characteristics of AlGaN/GaN MOSHEMTs with (a) planar channel, (b) 500-nm-wide fin-channel array, and (c) 300-nm-wide fin-channel array.

caused by the lateral electric field [21], [22]. The maximum extrinsic transconductance (g_{mmax}) was 85.8 mS/mm, 121.9 mS/mm, and 194.2 mS/mm for the devices with planar channel, 500-nm-wide channel array, and 300-nm-wide channel array, respectively. The improved g_{mmax} in the devices with a narrower fin-channel width was attributed to the better gate control capability and better heat dissipation in the narrower fin-channel structure.

The subthreshold swing (SS), defined as $dV_{GS}/d(\log I_{DS})$, was extracted from typical drain-source current-gate-source voltage (I_{DS}-V_{GS}) characteristics at $V_{DS} = 0.1$ V (Fig. 6). The SS of the devices with planar channel, 500-nm-wide channel array, and 300-nm-wide channel array was 380.2, 175.9, and 113.1 mV/dec, respectively. The improvement of SS by decreasing the fin-channel width was attributed to

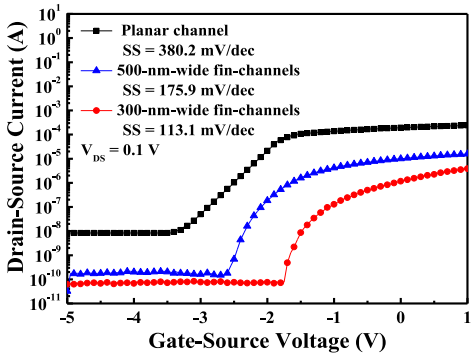

FIGURE 6. Typical drain-source current-gate-source voltage characteristics of various AlGaN/GaN MOSHEMTs operated at a drain-source voltage of 0.1 V.

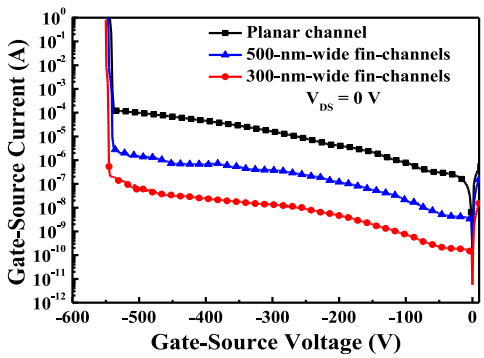

FIGURE 7. Dependence of gate-source leakage current on gate-source voltage of various AlGaN/GaN MOSHEMTs.

the better heat dissipation and better gate control capability in narrower fin-channel array [19]–[23]. Fig. 7 shows the dependence of gate-source leakage current on gate-source voltage. As shown in Fig. 7, it was found that the gate-source leakage current at a bias voltage of $V_{GS} = -100$ V was 778.2 nA, 20.4 nA and 0.73 nA for the devices with planar channel, 500-nm-wide channel array, and 300-nm-wide channel array, respectively. The smaller gate-source leakage current is attributed to the smaller real total gate area in the narrower fin-channel array. However, similar gate-source breakdown voltage of approximately −540 V was obtained for the different channel designs. The low gate-source leakage current and high gate-source breakdown voltage can verify the high quality and high insulation of the Ga_2O_3 films deposited by vapor cooling condensation system at low temperature.

Fig. 8 shows the small-signal high frequency characteristics of the various devices measured with a network analyzer (Agilent 8150C). The extrinsic unit gain cutoff frequency (f_T) and the maximum oscillation frequency (f_{max}) were 5.7 GHz and 11.0 GHz, 6.0 GHz and 13.2 GHz, and 6.4 GHz and 14.8 GHz for the AlGaN/GaN MOSHEMTs with planar channel, 500-nm-wide channel array, and 300-nm-wide channel array, respectively. Figs. 9(a), (b), and (c) show the normalized noise power density ($S_{I_{DS}}(f)/I_{DS}^2$) spectra as a function of frequency (f) of the various devices

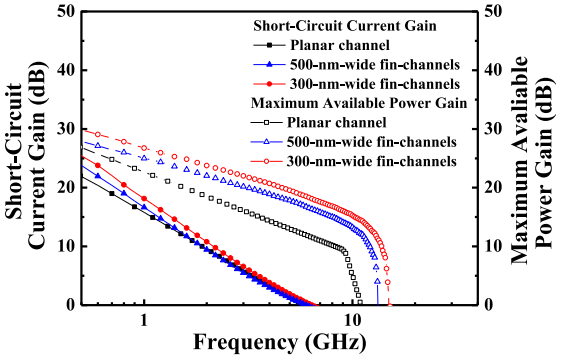

FIGURE 8. Short-circuit current gain and maximum available power gain as a function of frequency of various AlGaN/GaN MOSHEMTs.

TABLE 1. Comparison of Hooge's coefficient of various devices.

Material / Parameter	ZnO [26]	Ga_2O_3 [27]	SiO_2 [28]	Ni/Au Schottky [29]	Pt/Au Schottky [30]	This work
Hooge's coefficient	9.7×10^{-5}	1.0×10^{-3}	1.0×10^{-3}	1.6×10^{-3}	1.0×10^{-3}	5.1×10^{-5}

measured with a low-noise bias supply (Agilent 4156C semiconductor parameter analyzer), dynamic signal analyzer (HP 35670A), and noise analyzer (BTA 9812B) where S_{IDS} was the noise power density. The normalized noise power density at 1 Hz was $3.79 \times 10^{-14}Hz^{-1}$, $1.41 \times 10^{-14}Hz^{-1}$, and $8.45 \times 10^{-15}Hz^{-1}$ for the devices with planar channel, 500-nm-wide channel array, 300-nm-wide channel array, respectively. The normalized noise power density was reduced with narrower fin-channels owing to better screening effect of trapping/detrapping probability [24]. To compare low-frequency noise performances, the Hooge's coefficient α is a figure-of-merit of devices. Using the mobility fluctuation model [25], the α value is calculated from the following expression:

$$\alpha = \left(S_{I_{DS}}(f)/{I_{DS}}^2\right) \cdot f \cdot (L_G W_G n_{ch}(V_{GS} - V_T)/|V_T|) \quad (1)$$

where f is frequency, L_G is gate length, W_G is gate width, n_{ch} is channel electron density, V_{GS} is gate-source voltage, and V_T is threshold voltage. By substituting the related values, under the operation of $V_{DS} = 1$ V and f = 100 Hz, the α value of 5.1×10^{-5}, 8.0×10^{-6}, and 6.2×10^{-6} was obtained for the devices with planar channel, 500-nm-wide channel array, and 300-nm-wide channel array, respectively. To compare the low-frequency noise performances with the other published results, Table 1 listed the Hooge's coefficient of various devices. It was found that the better low-frequency noise performances were achieved by using the Ga_2O_3 films deposited using the vapor cooling condensation system. Furthermore, by extracting the normalized noise power density as a function of $1/f^{\gamma}$ shown in Fig. 9, the γ value was approximately 1. This phenomenon indicated that the flick noise was the dominant noise.

IV. SUMMARY AND CONCLUSION

To summarize the features of Ga_2O_3-gate-structured fin-channel width, Table 2 listed the figures of merit of the

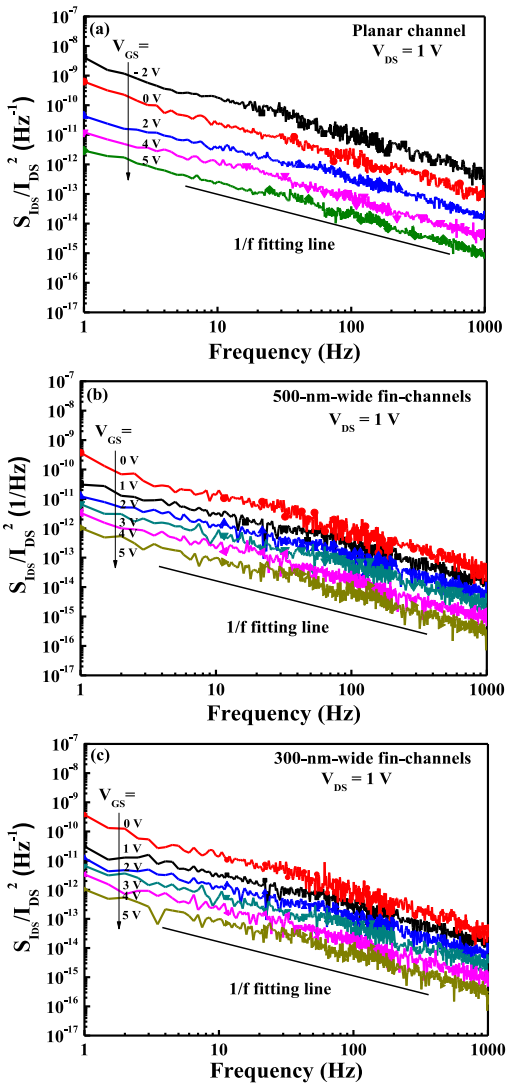

FIGURE 9. Normalized noise power density spectra as a function of frequency under a bias drain-source voltage of 1 V of the AlGaN/GaN MOSHEMTs with (a) planar channel, (b) 500-nm-wide channel array, and (c) 300-nm-wide channel array.

AlGaN/GaN MOSHEMTs with Ga_2O_3-gate insulator layer and with planar channel, 500-nm-wide fin-channel array, and 300-nm-wide fin-channel array, respectively. It was found that the performances were improved by reducing the width of fin-channel array. Since the efficient heat dissipation was better by driving lateral heat flow in a narrower fin-channel array [19], [20], the normalized saturation drain-source current and maximum extrinsic transconductance were consequently improved. Furthermore, owing to the early pinch-off effect [22], the threshold voltage in the AlGaN/GaN MOSHEMTs with a narrower fin-channel array was pushed toward a more positive voltage. That the subthreshold swing reduced with a narrower fin-channel width was attributed to the better heat dissipation driven by a lateral heat flow, better gate control capability, and effective passivation by Ga_2O_3 film [19]–[23]. Besides, in

TABLE 2. Performances of various-structured GaN-based MOSHEMTs with Ga_2O_3 gate insulator layer.

Channel structure	Planar channel channel width = 50 μm	Fin-channel array (channel width (nm))	
		500	300
Normalized saturation drain-source current (mA/mm) at V_{DS} = 10 V and V_{GS} = 5 V	506.7	617.6	750.0
Maximum extrinsic transconductance (mS/mm)	85.8	121.9	194.2
Threshold voltage (V)	−3.5	−2.3	−1.4
Subthreshold voltage (mV/dec)	380.2	175.9	113.1
Extrinsic unit gain cutoff frequency (GHz)	5.7	6.0	6.4
Maximum oscillation frequency (GHz)	11.0	13.2	14.8
Normalized noise power density (Hz^{-1})	3.79×10^{-14}	1.41×10^{-14}	8.45×10^{-15}
Hooge's coefficient	5.1×10^{-5}	8.0×10^{-6}	6.2×10^{-6}

view of the better gate control capability and the better complete separation between 2-DEG channel layer and GaN buffer layer in the narrower fin-channel region, the low-noise performances were consequently improved by reducing the width of fin-channel array owing to the better screening effect of trapping/detrapping probability [24]. Because of the smaller real total gate area in the AlGaN/GaN MOSHEMTs with narrower fin-channel array, the resulted smaller parasitic parameters improved the high frequency performances. Besides, the obtained low gate-source leakage current and high gate-source breakdown voltage verified that high quality and high insulating Ga_2O_3 films were achieved using the deposition of vapor cooling condensation system. AlGaN/GaN fin-MOSHEMTs with a Ga_2O_3 gate insulator deposited by the novel vapor cooling condensation system is a promising candidate in high-power and high-frequency applications.

REFERENCES

[1] K. J. Chen *et al.*, "GaN-on-Si power technology: Devices and applications," *IEEE Trans. Electron Devices*, vol. 64, no. 3, pp. 779–795, Mar. 2017, doi: 10.1109/TED.2017.2657579.

[2] U. K. Mishra, L. Shen, T. E. Kazior, and Y.-F. Wu, "GaN-based RF power devices and amplifiers," *Proc. IEEE*, vol, 96, no. 2, pp. 287–305, Feb. 2008, doi: 10.1109/JPROC.2007.911060.

[3] Y.-L. Chiou and C.-T. Lee, "Band alignment and performance improvement mechanisms of chlorine-treated ZnO-gate AlGaN/GaN metal–oxide–semiconductor high-electron mobility transistors," *IEEE Trans. Electron Devices*, vol. 58, no. 11, pp. 3869–3875, Nov. 2011, doi: 10.1109/TED.2011.2163721.

[4] A. Mohanbabu, N. Mohankumar, D. G. Raj, P. Sarkar, and S. K. Saha, "Efficient III-nitride MIS-HEMT devices with high-k gate dielectric for high-power switching boost converter circuits," *Superlattices Microstruct.*, vol. 103, pp. 270–284, Mar. 2017, doi: 10.1016/j.spmi.2017.01.043.

[5] C.-T. Lee, C.-L. Yang, C.-Y. Tseng, J.-H. Chang, and R.-H. Horng, "GaN-based enhancement-mode metal-oxide-semiconductor high-electron mobility transistors using $LiNbO_3$ ferroelectric insulator on gate-recessed structure," *IEEE Trans. Electron Devices*, vol. 62, no. 8, pp. 2481–2487, Aug. 2015, doi: 10.1109/TED.2015.2446990.

[6] S. J. Pearton *et al.*, "A review of Ga_2O_3 materials, processing, and devices," *Appl. Phys. Rev.*, vol. 5, no. 1, Jan. 2018, Art. no. 011301, doi: 10.1063/1.5006941.

[7] H.-C. Chiu, J.-H. Wu, C.-W. Yang, F.-H. Huang, and H.-L. Kao, "Low-frequency noise in enhancement-mode GaN MOS-HEMTs by using stacked $Al_2O_3/Ga_2O_3/Gd_2O_3$ gate dielectric," *IEEE Electron Device Lett.*, vol. 33, no. 7, pp. 958–960, Jul. 2012, doi: 10.1109/LED.2012.2194980.

[8] H.-Y. Lee, J.-T. Liu, and C.-T. Lee, "Modulated Al_2O_3-alloyed Ga_2O_3 materials and deep ultraviolet photodetectors," *IEEE Photon. Technol. Lett.*, vol. 30, no. 6, pp. 549–552, Mar. 2018, doi: 10.1109/LPT.2018.2803763.

[9] C.-H. Lin and C.-T. Lee, "Ga_2O_3-based solar-blind deep ultraviolet light-emitting diodes," *J. Lumin.*, vol. 224, Aug. 2020, Art. no. 117326, doi: 10.1016/j.jlumin.2020.117326.

[10] K. J. Chen *et al.*, "Surface nitridation for improved dielectric/III-nitride interfaces in GaN MIS-HEMTs," *Phys. Status Solidi A*, vol. 212, no. 5, pp. 1059–1065, May 2015, doi: 10.1002/pssa.201431712.

[11] H. Shen *et al.*, "Growth and characterization of β-Ga_2O_3 thin films by sol-gel method for fast-response solar-blind ultraviolet photodetectors," *J. Alloy Compounds*, vol. 766, pp. 601–608, Oct. 2018, doi: 10.1016/j.jallcom.2018.06.313.

[12] R. Wakabayashi, K. Yoshimatsu, M. Hattori, and A. Ohtomo, "Epitaxial structure and electronic property of β-Ga_2O_3 films grown on MgO (100) substrates by pulsed-laser deposition," *Appl. Phys. Lett.*, vol. 111, no. 16, Oct. 2017, Art. no. 162101, doi: 10.1063/1.4990779.

[13] D. Y. Guo *et al.*, "Fabrication of β-Ga_2O_3 thin films and solar-blind photodetectors by laser MBE technology," *Opt. Mater. Exp.*, vol. 4, no. 5, pp. 1067–1076, May 2014, doi: 10.1364/OME.4.001067.

[14] D. Y. Guo *et al.*, "Oxygen vacancy tuned Ohmic-Schottky conversion for enhanced performance in β-Ga_2O_3 solar-blind ultraviolet photodetectors," *Appl. Phys. Lett.*, vol. 105, no. 2, Jul. 2014, Art. no. 023507, doi: 10.1063/1.4890524.

[15] Y.-L. Chiou, L.-H. Huang, and C.-T. Lee, "Photoelectrochemical function in gate-recessed AlGaN/GaN metal–oxide–semiconductor high-electron-mobility transistors," *IEEE Electron Device Lett.*, vol. 31, no. 3, pp. 183–185, Mar. 2010, doi: 10.1109/LED.2009.2037983.

[16] Y. J. Lin, C. D. Tsai, Y. T. Lyu, and C. T. Lee, "X-ray photoelectron spectroscopy study of $(NH_4)_2S_x$-treated Mg-doped GaN layers," *Appl. Phys. Lett.*, vol. 77, no. 5, pp. 687–689, Jul. 2000, doi: 10.1063/1.127086.

[17] H. Y. Lee, S. D. Xia, W. P. Zhang, L. R. Lou, J. T. Yan, and C. T. Lee, "Mechanisms of high quality i-ZnO thin films deposition at low temperature by vapor cooling condensation technique," *J. Appl. Phys.*, vol. 108, no. 7, Oct. 2010, Art. no. 073119, doi: 10.1063/1.3477325.

[18] H.-Y. Lee, C.-H. Lin, and C.-T. Lee, "Whole metal oxide p-i-n deep ultraviolet light-emitting diodes using i-Ga_2O_3 active emissive film," *IEEE Photon. Technol. Lett.*, vol 32, no. 15, pp. 941–943, Aug. 2020, doi: 10.1109/LPT.2020.3003594.

[19] J. T. Asubar, Z. Yatabe, and T. Hashizume, "Reduced thermal resistance in AlGaN/GaN multi-mesa-channel high electron mobility transistors," *Appl. Phys. Lett.*, vol. 105, no. 5, Aug. 2014, Art. no. 053510, doi: 10.1063/1.4892538.

[20] M. Mikulics *et al.*, "Efficient heat dissipation in AlGaN/GaN heterostructure grown on silver substrate," *Appl. Mater. Today*, vol. 7, pp. 134–137, Jun. 2017, doi: 10.1016/j.apmt.2017.02.008.

[21] B. Lu, E. Matioli, and T. Palacios, "Tri-gate normally-off GaN power MISFET," *IEEE Electron Device Lett.*, vol. 33, no. 3, pp. 360–362, Mar. 2012, doi: 10.1109/LED.2011.2179971.

[22] K.-S. Im, Y.-W. Jo, J.-H. Lee, S. Cristoloveanu, and J.-H. Lee, "Heterojunction-free GaN nanochannel FinFETs with high performance," *IEEE Electron Device Lett.*, vol. 34, no. 3, pp. 381–383, Mar. 2013, doi: 10.1109/LED.2013.2240372.

[23] J.-J. Jia, C.-C. Lin, and C.-T. Lee, "Scaling effect in gate-recessed AlGaN/GaN fin-nanochannel array MOSHEMTs," *IEEE Access*, vol. 8, pp. 158941–158946, 2020, doi: 10.1109/ACCESS.2020.3020316.

[24] S. Vodapally *et al.*, "Comparison for 1/f noise characteristics of AlGaN/GaN FinFET and planar MISHFET," *IEEE Trans. Electron Devices*, vol. 64, no. 9, pp. 3634–3638, Sep. 2017, doi: 10.1109/TED.2017.2730919.
[25] F. N. Hooge, T. G. M. Kleinpenning, and L. K. J Vandamme, "Experimental studies on 1/f noise," *Rep. Progr. Phys.*, vol. 44, no. 5, pp. 479–532, 1981, doi: 10.1088/0034-4885/44/5/001.
[26] C.-T. Lee, Y.-L Chiou, and C.-S. Lee, "AlGaN/GaN MOS-HEMTs with gate ZnO dielectric layer," *IEEE Electron Device Lett.*, vol. 31, no. 11, pp. 1220–1223, Nov. 2010, doi: 10.1109/LED.2010.2066543.
[27] H.-Y. Shih, F.-C. Chu, A. Das, C.-Y. Lee, M.-J. Chen, and R.-M. Lin, "Atomic layer deposition of gallium oxide films as gate dielectrics in AlGaN/GaN metal–oxide–semiconductor high-electron-mobility transistors," *Nanoscale Res. Lett.*, vol. 11, p. 235, Apr. 2016, doi: 10.1186/s11671-016-1448-z.
[28] Y.-Z. Chiou, "Noise analysis of AlGaN/GaN metal-oxide-semiconductor heterostructure field effect transistors with photochemical-vapor deposition SiO_2 layers," *Jpn. J. Appl. Phys.*, vol. 44, no. 4S, pp. 2465–2468, Apr. 2005, doi: 10.1143/JJAP.44.2465.
[29] S. K. Jha, C. Surya, K. J. Chen, K. M. Lau, and E. Jelencovic, "Low-frequency noise properties of double channel AlGaN/GaN HEMTs," *Solid-State Electron.*, vol. 52, no. 5, pp. 606–611, May 2008, doi: 10.1016/j.sse.2007.10.002.
[30] N. Pala *et al.*, "Low frequency noise in AlGaN/InGaN/GaN double heterostructure field effect transistors," *Solid-State Electron.*, vol. 47, no. 6, pp. 1099–1104, Jun. 2003, doi: 10.1016/S0038-1101(02)00475-6.